Supplementary Information: Full-Range Front Criteria for Generalized van Genuchten–Mualem Laws, with Finite-Head Applications

Kyungdoe Han

This Supplement gives the complete assumptions and proofs, the detailed fitting and interval-bound calculations, and additional exact-front examples. Van Genuchten–Mualem is abbreviated VGM. Supplementary labels carry the prefix S, and an unprefixed reference points to the article unless a local label has the same name.

The following notation is used throughout. The effective saturation is $s \in [0, 1]$, the depth is z, and the time is t. The storage-normalized diffusivity is D and the storage-normalized hydraulic conductivity is K. The straight line joining the conductivities at the selected endpoints is L, and $G = L - K$ is the gap between that line and the conductivity curve. The function Q gives profile position as a function of the cumulative saturation-change level $p \in (0, 1)$, and $\rho = -U'$ is the profile slope magnitude. A prime denotes differentiation with respect to the shown scalar argument.

Contents

S1 Auxiliary exact front extensions

Two subsections connect the representation to practical settings. The first recovers a known closed-form front and measures that recovery, and the second separates the chord procedure from three simpler tests. Neither alters the VGM classifications in the article.

S1.1 Closed-form recovery benchmark

Prescribing compatible hydraulic functions to obtain an exact traveling front is an established verification (Zlotnik et al., 2007; Broadbridge and White, 1988; Caputo and Stepanyants, 2008). One elementary member of that construction measures the recovery chain here. The cubic front is recovered with $K_\mathrm{d} = 0$, $c = K_s$,

$$D(s) = D_0(1-s), \qquad G(s) = K_s s(1-s)^2, \qquad \kappa = K_s/D_0. \tag{S1}$$

The symbol κ is local to this benchmark and is unrelated to the retention scale α. Then $D/G = 1/[\kappa s(1-s)]$, so

$$K(s) = K_s s - G(s) = K_s s^2(2-s), \qquad S(z,t) = \frac{1}{1+\exp[\kappa(z - K_s t - z_0)]}, \qquad j = K_s S. \tag{S2}$$

The resulting profile is one fixed-conductivity logistic member of the general construction. Symbolic substitution of S into $S_t = \partial_z[D(S)S_z - K(S)]$ returns zero, so the closed form is a solution of the Richards equation independently of the construction being tested.

The numerical check starts from D and G alone. It integrates $Q'(p) = D(1-p)/G(1-p)$ from $p = 1/2$, inverts the resulting monotone quantile, and compares the recovered profile with the closed form. Nothing in the chain uses $Q(p) = \kappa^{-1}\log\{p/(1-p)\}$, so the comparison is a test rather than an identity. Table S1 sets $D_0 = K_s = 1$ and reports fixed-order quadrature convergence.

Table S1: Gauss–Legendre quadrature of the quantile derivative converges to the exact logistic quantile. Entries through order 64 are maximum absolute errors over 49 logit-spaced levels from -6 to 6. The order-128 entry is a conservative upper bound across double-precision replays.

Gauss–Legendre order	Maximum error
16	5.3×10^{-2}
32	6.3×10^{-4}
64	7.8×10^{-8}
128	$\leq 9.0 \times 10^{-13}$

The staged and independent replays give 8.6×10^{-13} and 5.1×10^{-13} at order 128, both below the reported bound.

Adaptive quadrature at tolerance 10^{-13} reduces the maximum quantile error to 1.2×10^{-14}. Inverting that quantile on $-8 \leq \xi \leq 8$ gives a maximum profile error of 4.9×10^{-16}, consistent with double-precision roundoff. Using the 128-point values instead gives 3.3×10^{-9}, so the reported reconstruction error is controlled by quadrature. Because the profile is defined as the inverse of the integral of D/G, a residual of that same first-order relation would not provide an independent verification.

S1.2 Direct comparison with simpler procedures

The comparison cases use standard VGM with $m = 1/2$ and $n = 2$, for which the Mualem integral is elementary. Written without dry-end cancellation,

$$A(s) = \frac{s^2}{1+\sqrt{1-s^2}}, \qquad k_r(s) = \frac{s^{l+4}}{\left(1+\sqrt{1-s^2}\right)^2}, \qquad A'(s) = \frac{s}{\sqrt{1-s^2}}. \tag{S3}$$

This form agrees with the regularized incomplete-beta evaluation used for the certificates to within 2.2×10^{-76} on $[0.01, 0.99]$, so the elementary shortcut cannot hide a transcription error. Every value below is an outward-rounded enclosure at 256 bits, and each classification repeats at 384 bits. Table S2 collects the four cases.

Table S2: Each case separates the chord procedure from one simpler test. Directed rounding encloses every reported sign.

Simpler test	Parameters	Enclosed result	Consequence
Monotonicity	$l = -3.5$	Here $l + 4 = 1/2 > 0$, so s^{l+4} increases while $(1 + \sqrt{1-s^2})^2$ decreases. Also $k_r'(0.01) > 1.25031$ and the chord gap at 0.01 is below -0.0150012.	Conductivity increases across the open interval yet crosses above the endpoint chord.
Finite grid	$l = -3.01$	All 5,999 interior grid gaps are positive, and the smallest lower bound is 4.83×10^{-8}. The chord crossing lies at $6.2230152778611417 \times 10^{-61}$.	Sampled positivity does not certify the open interval, even on an endpoint-clustered grid.
Full-endpoint label	$l = -3.5$, $S_{\mathrm{cap}} = 0.1$	Supported by a 27-cell cover, with cap speed enclosed at 1.0228280953 and smallest interior gap bound 3.84×10^{-4}.	Endpoint reselection can support a capped front that the full endpoint pair excludes.
Clipping	$l = -2$, $S_{\mathrm{cap}} = 0.1$	The cap speed is 1.1083193570 rather than 1. At $s = 0.5$ the cap gap minus the full gap is -0.05415967851.	A clipped full profile carries the wrong speed and solves a different first-order profile equation.

The first interior state of the endpoint-clustered grid is 6.85389×10^{-8}, which exceeds the crossing state of the finite-grid case by a factor above 10^{53}. At that crossing, the unrationalized form $A(s) = 1 - \sqrt{1-s^2}$ evaluates to exactly zero in double precision, so a direct evaluation reports the gap as positive as well.

S2 VGM fitting and finite-cap classification

The public-data application locates analytical classes in fitted parameter space rather than observing fronts. The procedures below specify fitting, curve inclusion, parameter identification, and finite-cap classification. Neither fitting nor curve inclusion uses the chord margin.

S2.1 Data windows, weights, and fitted formulations

Records are matched within each source by the source-specific sample identifier. The retained data include finite retention observations with $\mathrm{pF} \leq 4.2$ and finite conductivity observations with $\mathrm{pF} \leq 3.5$, where $\mathrm{pF} = \log_{10} |h/\mathrm{cm}|$. Eligibility also requires at least six distinct retention levels and four distinct conductivity levels. EU-HYDI record `EUHYDI_2760059020.0` is excluded because its normalized water-content field reaches 5.072 and the source transformation cannot be reconstructed. Applying the unit and observation-count rules leaves 1,791 records.

Both fitting stages use pF-interval weights to prevent densely sampled regions from dominating a curve. After sorting $x_1 \leq \cdots \leq x_N$, each endpoint receives half its adjacent spacing and each interior level receives half the sum of its two adjacent spacings. Division by the mean normalizes the weights. A zero spacing is replaced by 10^{-6} times the smallest positive spacing in the same record, which retains repeated levels without assigning zero weight.

The fitted retention curve is

$$\widehat{\theta}(x) = \theta_r + (\theta_s - \theta_r)\,[1 + \{10^x \alpha\}^n]^{-m}\,. \tag{S4}$$

The standard fit imposes $m = 1 - 1/n$, whereas the independent-shape fit estimates m and n separately. Both fits use $-6 \leq \log_{10} \alpha \leq 2$. The standard range is $1.01 \leq n \leq 20$, and the independent range is $0.05 \leq m \leq 0.95$ with $1.02 \leq n \leq 20$. The standard law is the analytical special case $m = 1 - 1/n$ of the independent-shape law, so the model families are nested. The imposed boxes are not. A standard point lies inside the independent-shape box only when $n \geq 1/0.95$, and 11 of the 1,508 paired retained records have a standard m below 0.05. The smallest standard m among the 14 class-changing records is 0.125, so no reported class change lies in the region where the boxes differ. The comparison is nonetheless not a formal nested-model test. At each nonlinear iterate, an exact box-constrained weighted least-squares calculation solves for (θ_r, θ_s) by enumerating the interior solution, all solutions with one active bound, and all corners. The bounds are

$$0 \leq \theta_r \leq \max\{10^{-8}, \min(0.70, \min_i \theta_i - 10^{-7})\}, \tag{S5}$$

$$\max_i \theta_i + 10^{-7} \leq \theta_s \leq \max\{1.2, \max_i \theta_i + 0.05 + 10^{-7}\}. \tag{S6}$$

The standard nonlinear problem begins on a fixed coarse grid and is refined by bounded limited-memory quasi-Newton optimization, abbreviated L-BFGS-B (Byrd et al., 1995). The independent problem uses the projected standard solution and four additional fixed starts. Candidates whose objectives differ by no more than a relative tolerance of 10^{-10} are treated as ties. Selection then favors successful optimizer termination, followed by deterministic objective and parameter tie breakers. If the selected candidate lacks a successful termination flag, a bounded Powell refinement (Powell, 1964) is added before final selection. The procedure uses neither random starts nor random resampling.

After retention is fixed, measured conductivity is linear in $(\log_{10} \mathcal{K}_s, l)$.

$$\log_{10} \widehat{\mathcal{K}}(x) = \log_{10} \mathcal{K}_s + l \log_{10} S(x) + 2 \log_{10} A\{S(x)\}. \tag{S7}$$

The factor A equals A_m for standard VGM and $I_{S^{1/m}}(m + 1/n, 1 - 1/n)$ for the independent-shape model. The same exact two-variable active-set solver is used with $-12 \leq \log_{10} \mathcal{K}_s \leq 8$ and $-30 \leq l \leq 15$. For the leave-one-observation-out summary, one conductivity observation is removed at a time. The omission unit is the observation rather than the pressure level, so a replicate at the same head can remain in the training set. The pair $(\mathcal{K}_s, l)$ is then refitted to the remaining observations after recomputing the pF-interval weights on the reduced set. The held-out residual $r_i = \log_{10} \mathcal{K}_i - \log_{10} \widehat{\mathcal{K}}_i$ defines the weighted root-mean-square error

$$\mathrm{RMSE}_w = \left(\frac{\sum_i w_i r_i^2}{\sum_i w_i} \right)^{1/2} \tag{S8}$$

under the weights of the complete curve. Retention parameters remain fixed at their all-retention estimates.

Several features limit the interpretation of this diagnostic. A single observation is omitted, so a companion measurement at the same pF level remains in the training set. Replicated pF levels account for 3.4 percent of the retained conductivity observations. Only $(\mathcal{K}_s, l)$ are refitted, which makes the diagnostic a test of conductivity-level reconstruction with retention held fixed rather than out-of-sample validation of the complete constitutive law. The eligibility screen and inclusion R^2 use unweighted residuals, whereas (S8) is weighted. Every conductivity value in the normalized set is strictly positive, so the logarithm requires no censoring or substitution for zero, negative, or below-detection values.

S2.2 Curve inclusion and parameter identification

The inclusion rules first identify retention and conductivity curves that meet the stated fit criteria. Front classes are compared only within that set, after which separate diagnostics identify independent-shape fits that are weakly constrained.

A curve is included when its retention RMSE is at most 0.04 and its retention R^2 is at least 0.75. The same curve must have log-conductivity RMSE at most one decade and log-conductivity R^2 at least 0.50. The same thresholds apply to both formulations, and the full-range class does not enter either threshold. The thresholds retain 1,539 standard fits and 1,548 independent-shape fits, including 1,508 records retained under both formulations. All 1,791 independent fits select a successfully terminated L-BFGS-B result, and no final record uses the Powell fallback. Because the retention objective is nonconvex, successful termination establishes only that the best tested start met a local convergence criterion.

The 14 records that change full-range class were refitted from 257 deterministic starts. The five initial values used in the reported fit are the projected standard solution and four fixed points in $(\log_{10} \alpha, \log m, \log(n-1))$. They are $(-1, \log 0.5, \log 1)$, $(-2, \log 0.2, \log 2)$, $(0, \log 0.8, \log 0.5)$, and $(-4, \log 0.1, \log 7)$. A $7 \times 6 \times 6$ grid adds 252 starts on the parameter box, spaced uniformly in the same coordinates. Every start is attempted, and solutions are grouped after rounding each coordinate to six decimals. The scaled objective increase is the objective minus the smallest one found, divided by one plus that value. For every record, the lowest-objective solution found gave the same result as the reported fit, and the objective decreased by at most 5.6×10^{-15}. The tested starts found no lower objective with a different class. This search does not establish global optimality.

The search also returned other converged retention solutions. Each was reclassified by refitting $(\mathcal{K}_s, l)$ to the conductivity observations for that retention solution, because a different retention solution changes the saturations and therefore the fitted exponent. Four records have solutions on both sides of the chord boundary. They are UNSODA 4700 and EU-HYDI 2760052001, 2760052605, and 3800085502. For each record, the smallest scaled objective increase that admits an opposite-class solution is 1.0×10^{-5}, 2.6×10^{-6}, 4.2×10^{-6}, and 1.5×10^{-4}. In each record, that first observed crossover solution also meets all four common quality thresholds. Twelve of the 99 opposite-class solutions meet them. The sensitivity therefore survives the inclusion rule among the tested converged solutions within the stated objective range. It does not require the selected optimum to lie near the boundary, since UNSODA 4700 has a selected margin of 1.30. The band summarizes variation among the tested converged solutions and has no sampling-based coverage interpretation.

Table S3: The four records with converged solutions on both sides of the chord boundary. The margin range uses scaled objective increases no greater than 10^{-3}. Distinct counts include all converged solutions from 257 starts. Active bounds and conductivity diagnostics describe the first observed crossover solution after conductivity refitting.

Record	Selected class, margin	Smallest increase	Margin range	Distinct	Opposite passing	Active bounds	$\mathrm{RMSE}_{\log K}$	$R^2_{\log K}$
UNSODA 4700	supported, 1.2984	1.04×10^{-5}	$[-0.118, 5.19]$	228	2	none	0.168	0.882
EU-HYDI 2760052001	excluded, -0.1470	2.59×10^{-6}	$[-0.147, 12.43]$	139	5	none	0.070	0.925
EU-HYDI 2760052605	supported, 0.0745	4.19×10^{-6}	$[-0.434, 2.22]$	223	2	m	0.142	0.809
EU-HYDI 3800085502	excluded, -1.2128	1.53×10^{-4}	$[-1.213, 5.63]$	88	3	none	0.091	0.856

The EU-HYDI specification defines water content as water volume per soil volume (Weynants et al., 2013). Record `EUHYDI_2760059020.0` contains 42 normalized retention observations. Its maximum is 5.072, while the final three values are 0.010, 0.004, and 0.010. The normalized set provides no source-level unit or transformation lineage that resolves this mixed scale. The record is therefore excluded before fitting. This exclusion changes the fit-eligible count from 1,792 to 1,791 but does not change the 1,508 paired records or the cap summaries.

The storage range does not enter the dimensionless chord condition directly. Changing a water-content endpoint can still alter the normalized saturations, and therefore the fitted retention parameters, the Mualem integral, and the refitted conductivity exponent. The range also sets $\Delta W = \theta_s - \theta_r$ and hence the dimensional front speed.

For each independent fit, a centered finite-difference Hessian of the profiled retention objective is computed in $(\log_{10} \alpha, \log m, \log(n-1))$ with step 0.002. The objective is profiled in the sense that the two water-content endpoints are solved exactly at each nonlinear iterate, so only the nonlinear parameters remain. For an interior fit with a positive definite Hessian, the spectral condition number is the ratio of the largest eigenvalue to the smallest. A large value means the objective is nearly flat in some direction. A fit with a nonpositive eigenvalue is reported separately as indefinite or numerically singular. The condition number is used only as a local identification diagnostic, while a separate flag records contact with the stated α, m, or n bounds. Among the paired fits, 932 reach one of those bounds, which is 61.8 percent of the total, and 71 have a Hessian condition number above 10^6. Of these 71 fits, 36 also lie on an active retention bound and 35 are interior. At an active bound, the centered finite-difference stencil extends outside the feasible box and does not represent the local curvature of the constrained problem. The 36 associated condition numbers are therefore treated as flags rather than calibrated identification measures. One additional record returns a numerically singular Hessian.

Figure S1 shows the paired chord margins with the shape-parameter bound contacts marked, together with the held-out log-conductivity error by source. Both are diagnostics of the fitting rather than steps in the front argument.

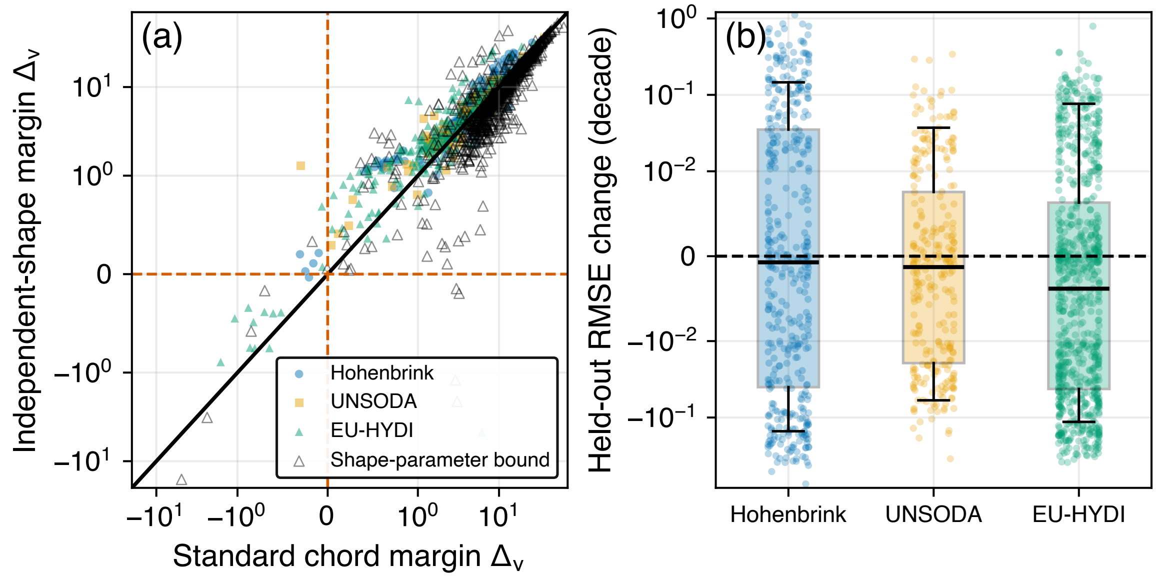

Figure S1: (a) Standard against independent-shape chord margin for the 1,508 paired records, with source encoded by marker and open triangles marking fits at a shape-parameter bound. (b) Change in held-out log-conductivity error, independent shape minus standard, by source.

Table S4 gives the paired full-range classifications.

Table S4: Paired full-range classifications for the 1,508 records retained under both VGM formulations.

	Independent outside	Independent inside
Standard outside	15	9
Standard inside	5	1,479

Excluding every retention or conductivity bound hit under either model leaves 569 records. In the row and column order used in Table S4, the four cells are 11, 7, 1, and 550. Eight of the 14 direction changes remain because this screen targets the parameters that enter the chord formula. A stricter screen also excludes active θ_r and θ_s bounds. The stricter screen retains 98 records, with cells 3, 1, 1, and 93 in the same order. Each model then has 94 passes, and two direction changes remain.

S2.3 Interval certification of every cap classification

Positive classification asserts that the secant gap stays positive across the whole open state interval. A sampled root list cannot establish that, so every supported case is proved by an adaptive interval cover with outward-rounded arithmetic (Moore et al., 2009; Johansson, 2017). Outward rounding sends each lower bound down and each upper bound up, so every enclosure retains the exact value. Each cell is discharged by one of three rules.

An interior cell is discharged when the lower bound of the enclosed gap is positive. The gap vanishes at both endpoints by construction, so the two endpoint cells are discharged by monotonicity instead. At the dry end a positive lower bound on the gap derivative makes the gap positive immediately to the right of the selected dry endpoint. At the wet end a positive lower bound on

k_r' that exceeds the reduced secant speed makes the gap decreasing, hence positive just below its return to zero. A natural interval extension is unusable there, because k_r' diverges as $s \to 1$, so the wet cell uses a closed-form bound instead.

Both formulations share one implementation, because the Mualem integral is the regularized incomplete beta function $A(s) = I_{s^{1/m}}(a_\beta, b_\beta)$ with $a_\beta = m + 1/n$ and $b_\beta = 1 - 1/n$ at $(\beta, \nu) = (1, 2)$. The symbol B denotes the beta function. Its derivative is

$$A'(s) = \frac{s^{1/(mn)}\left(1 - s^{1/m}\right)^{-1/n}}{mB(a_\beta, b_\beta)}, \qquad k_r'(s) = ls^{l-1}A(s)^2 + 2s^l A(s)A'(s). \tag{S9}$$

Both variable factors of A' increase toward one, so on a wet cell $[\sigma, 1)$,

$$A'(s) \geq \Lambda_\mathrm{w} := \frac{\sigma^{1/(mn)}\left(1 - \sigma^{1/m}\right)^{-1/n}}{mB(a_\beta, b_\beta)}. \tag{S10}$$

With $A \leq 1$ this gives

$$k_r'(s) \geq \begin{cases} 2\sigma^l A(\sigma)\Lambda_\mathrm{w}, & l \geq 0, \\ l\sigma^{l-1} + 2A(\sigma)\Lambda_\mathrm{w}, & l < 0, \end{cases} \qquad s \in [\sigma, 1). \tag{S11}$$

For $l \geq 0$ both factors s^l and $A(s)$ increase. For $l < 0$ the negative first term uses $s^{l-1}A(s)^2 \leq \sigma^{l-1}$ and the positive term uses $s^l \geq 1$. The standard law is the case $n = (1 - m)^{-1}$, for which $a_\beta = 1$, $b_\beta = m$, and $B = 1/m$, so (S10) reduces to $A'(s) \geq (1 - \sigma^{1/m})^{m-1}\sigma^{1/m-1}$.

An exclusion needs no cover. One cell whose gap enclosure lies entirely below zero witnesses that the gap is not positive throughout. Complete root enumeration is therefore unnecessary for the excluded cases as well.

Near the wet endpoint the reflection $I_x(a, b) = 1 - I_{1-x}(b, a)$ gives the narrower enclosure. Finite decimal inputs are converted through exact rationals. For the standard law, $m = 1 - 1/n$ is derived from the fitted n. Each pressure endpoint is computed from α, m, n, and h_cap inside the interval calculation. A comparison that cannot be decided leaves the case unresolved rather than classified.

All 61 positive classifications are certified and all 119 exclusions carry a witness, so every one of the 180 combinations is decided. Repeating the whole calculation at twice the working precision, 600 bits against 300, returns the same status in every case. No certificate contradicts the reported classification.

Each certificate records the interval evidence rather than a verdict. Cells are exact dyadic intervals of the normalized state coordinate. They are mapped to state space by $s = S_\mathrm{cap} + (1 - S_\mathrm{cap})u$ without discarding the radius of S_cap. Integer arithmetic verifies that each cover is an ordered partition of the whole normalized interval.

These are fixed-parameter certificates. They prove the gap inequality at the stored fitted parameter values and do not propagate uncertainty in those parameters or storage endpoints. Parameter uncertainty would need interval parameter boxes or a boundary-distance calculation, which the affine margin supplies for the full-range class.

S2.4 Finite-cap computation and reproducibility checks

For each retained law outside the full-range class, Equation (S71) gives the cap floor. The dimensionless conductivity and its analytical derivative then determine the reduced secant speed and the stationary equation $k_r'(s) = \widehat{c}_{\mathrm{cap},1}$. Candidate stationary points are bracketed on the endpoint-clustered grid

$$s_j = S_{\mathrm{cap}} + (1 - S_{\mathrm{cap}}) \sin^2\left(\frac{j\pi}{12000}\right), \qquad j = 0, \ldots, 6000. \tag{S12}$$

Each sign-changing bracket is refined by a scalar solve. When the critical set is finite, Theorem S8 reduces endpoint classification to strict positivity of the gap at every stationary point. The search returns one or two roots for each of the 180 model and cap combinations. The conservative branch that rejects a record without a bracketed root is therefore never used.

Such a search can miss an even-multiplicity root, a flat critical interval, or two roots in one grid cell. The interval cover above therefore carries the classification. Three numerical checks reduce the risk for the remaining cases. First, repeating the search on a 2×10^5-point grid returns the same root count for all 180 combinations. Second, a Lipschitz exclusion test screens every cell without a sign change. If $M \geq \max |G''_{\mathrm{cap},1}|$ on a subinterval $[a, b]$ of width $\delta s = b - a$,

$$|G'_{\mathrm{cap},1}| \geq \min\{|G'_{\mathrm{cap},1}(a)|, |G'_{\mathrm{cap},1}(b)|\} - Mh \tag{S13}$$

on that subinterval, and a positive right-hand side excludes a root of any multiplicity. The implementation samples the analytic second derivative on the same grid and multiplies the sampled maximum by four. The bound excludes roots from all but at most 26 cells per record, whose combined width is at most 8.9×10^{-5} of the state interval. The calculation is a strong numerical screen rather than an interval-arithmetic certificate. Every unresolved cell lies beside an identified root or in an endpoint cell where the gap derivative diverges and the gap approaches zero from a known side. Third, 60-digit refinement of every bracketed root changes the smallest stationary gap by at most 1.5×10^{-13} in relative terms and leaves all 180 classifications unchanged. Together, the checks support reproducibility under the stated protocol, but they do not prove that every critical point was enumerated.

The classifications have unequal margins. The smallest stationary gap among supported fronts is 0.135, whereas the closest excluded case is the independent-shape record Hohenbrink TUBS_131. The stationary gap is $-5.2808917422 \times 10^{-7}$ at the 3×10^3 cm cap and is slightly more negative at the two larger caps. High-precision refinement confirms the negative sign to 25 significant figures, so the exclusion is not a consequence of double-precision roundoff. A missed stationary point cannot reverse this exclusion because one identified stationary point already has a negative gap. Completeness matters only for cases classified as supported. Because the gap magnitude is within about one order of the 5×10^{-8} endpoint-cancellation tolerance used below, the analysis reports this record as a near-boundary exclusion.

A separate dense-grid check evaluates the gap at all 6,001 points with a 5×10^{-8} endpoint-cancellation tolerance. The dense-grid decisions agree with the stationary-root decisions for all 180 model and cap combinations. A second check hashes observation vectors after sorting and rounding every (pF, θ) and $(\mathrm{pF}, \log_{10} \mathcal{K})$ pair to six or eight decimal places. No cross-source duplicate group appears at either precision. The hash screen detects repeated observation vectors but cannot establish distinct physical samples because the normalized set lacks authoritative site, horizon, and study metadata.

Two table conventions are essential for dimensional interpretation. The stored cap speed is the dimensionless reduced speed $\widehat{c}_{\mathrm{cap},1}$ rather than $c_{\mathrm{cap},1}$. The stored saturated conductivity is the measured $\mathcal{K}_s$ in cm per day, so a dimensional front speed requires division by $\Delta W = \theta_s - \theta_r$. The two storage endpoints are stored with the single-formulation fits rather than the paired table.

S3 Complete formal statements and proofs

Each result below is stated in full and then proved, and the article carries the operative form of every one of them. The supplementary proofs remain beside their statements above. Notation follows the article, so endpoint constants, affine margins, and cap quantities keep their stated definitions.

The formal statements use standard mathematical notation. Here $\mathbb{R}$ is the real line, and C^k denotes functions with k continuous derivatives. The space L^r holds functions whose rth absolute power has a finite integral, and $W^{1,r}$ holds functions whose first weak derivatives lie in L^r. A subscript "loc" restricts the requirement to bounded subsets. The phrase almost everywhere, abbreviated a.e., permits exceptions on a null set. The relation $f \sim g$ means $f/g \to 1$, the relation $f = \Theta(g)$ means that f/g stays between positive finite bounds, and $f = o(g)$ means $f/g \to 0$. The beta function is $B(a,b)$, and $x_+ = \max(x,0)$.

S3.1 General front representation

The three results in this subsection record established front machinery in the storage-normalized variables used by the article. The lemma below states the traveling first integral, the endpoint secant speed, and the affine flux. These identities are established for scalar convection–diffusion equations and for Richards fronts (Gilding, 1991; Gilding and Kersner, 1996, 2004; Caputo and Stepanyants, 2008). They are restated here to fix the normalization and the one-sided endpoint assumptions used by the VGM results.

Lemma S1 (Traveling first integral and chord deficit)**.** *Suppose $S(z,t) = U(\xi)$, $\xi = z - ct - z_0$, is a continuous decreasing traveling front with $U(-\infty) = 1$, $U(+\infty) = 0$, and with vanishing capillary flux at any infinite endpoint. Write $K(0) = K_{\mathrm{d}}$ and $K(1) = K_{\mathrm{w}}$. Then*

$$c = K_{\mathrm{w}} - K_{\mathrm{d}}, \qquad L(s) = K_{\mathrm{d}} + cs, \qquad D(U)U' = -G(U), \qquad G(s) := L(s) - K(s), \tag{S14}$$

and the normalized flux is $j = L(S)$. In physical variables,

$$c = \frac{\mathcal{K}(v_{\mathrm{w}}) - \mathcal{K}(v_{\mathrm{d}})}{\Delta W}, \qquad \mathcal{G}(v) = \mathcal{K}(v_{\mathrm{d}}) + c\{W(v) - W(v_{\mathrm{d}})\} - \mathcal{K}(v). \tag{S15}$$

The definitions also give $K \geq 0$ on $[0,1]$ exactly when $G \leq L$, and $K' \geq 0$ exactly when $G' \leq c$.

Proof of Lemma S1. Substitution into (2) and one integration give $D(U)U' = K(U) - cU - j_*$. Evaluation at the endpoint states gives $j_* = K(0)$ and $c = K(1) - K(0)$. Therefore $D(U)U' = K(U) - L(U) = -G(U)$ and $j = K - DU' = L(U)$. Multiplication by ΔW gives (S15). Finally, $K = L - G$ and $K' = c - G'$ prove the two equivalences. ☐

For Proposition S2, a weak solution satisfies

$$S \in C([0,T]; L^1_{\mathrm{loc}}(\mathbb{R})) \cap W^{1,1}_{\mathrm{loc}}(\mathbb{R} \times (0,T)),$$
$$j = K(S) - D(S)S_z \in L^1_{\mathrm{loc}},$$

and

$$\int_0^T \int_{\mathbb{R}} \{S\phi_t + j\phi_z\}\,\mathrm{d}z\,\mathrm{d}t + \int_{\mathbb{R}} S(z,0)\phi(z,0)\,\mathrm{d}z = 0 \tag{S16}$$

for every $\phi \in C_c^\infty(\mathbb{R} \times [0,T))$. The diffusivity may lack a finite endpoint limit where the front is constant. Equation (S19) therefore defines the capillary product through a continuous representative.

The representative vanishes on each endpoint plateau and keeps the flux j well defined without assigning an endpoint value to D.

The construction below is the Richards specialization of the stationary pseudo-inverse representation for scalar quasilinear parabolic equations (Jourdain and Reygner, 2013). Two elements are specific to the hydraulic setting. The denominator of the quantile derivative is the endpoint chord gap G, which is also the quantity that decides existence. The capillary product is defined on each endpoint plateau through the continuous representative $G(U)$, so no endpoint limit of D is needed.

Proposition S2 (Richards specialization of the stationary inverse-CDF representation)**.** *Fix $K_{\mathrm{d}}, c \in \mathbb{R}$, put $L(s) = K_{\mathrm{d}} + cs$, and suppose $G \in C([0,1])$ and $D \in C(0,1)$ satisfy*

$$D(s) > 0, \quad G(s) > 0 \quad (0 < s < 1), \qquad G(0) = G(1) = 0, \qquad \eta := D/G \in C(0,1). \tag{S17}$$

No endpoint limit of D is assumed because the van Genuchten–Mualem diffusivity $D = Kh'$ diverges at the wet endpoint for every $n > 1$. Requiring continuity on the closed state interval would therefore exclude the laws classified below and the fitted laws of Section S2. The weak formulation instead requires only the product $D(U)U'$, which Equation (S19) identifies with the finite quantity $-G(U)$. Set $K = L - G$ and define

$$Q(p) = \int_{1/2}^{p} \eta(1-r)\,\mathrm{d}r, \qquad 0 < p < 1. \tag{S18}$$

Let $a = \lim_{p\downarrow 0} Q(p)$ and $b = \lim_{p\uparrow 1} Q(p)$, allowing infinite limits. Then Q is strictly increasing from $(0,1)$ onto (a,b). Let $F = Q^{-1}$ on (a,b), extend $F = 0$ on $(-\infty, a]$ when a is finite and $F = 1$ on $[b, \infty)$ when b is finite, and put $U = 1 - F$. Then the following statements hold.

1. *U is continuous, nonincreasing, locally absolutely continuous, and*

$$D(U)U' = -G(U), \qquad K(U) - D(U)U' = L(U) \tag{S19}$$

almost everywhere. The first identity holds pointwise on the open transition interval, where $D(U)$ is finite. On an endpoint plateau, $U' = 0$ and $G(U) = 0$, so the capillary flux $-D(U)U'$ is defined through the continuous representative $G(U)$ and continued by zero. Hence for every $z_0 \in \mathbb{R}$, $S(z,t) = U(z - ct - z_0)$ is a weak solution of (2). The traveling solution is classical wherever $0 < S < 1$.

2. *$\rho = -U' = F'$ is a probability density on the transition support, with CDF F and quantile Q.*

3. *The transition reaches neither endpoint at a finite coordinate exactly when*

$$\int_0^{1/2} \frac{D(s)}{G(s)}\,\mathrm{d}s = \infty, \qquad \int_{1/2}^{1} \frac{D(s)}{G(s)}\,\mathrm{d}s = \infty. \tag{S20}$$

When one integral is finite, the corresponding constant extension is the conservative weak completion.

4. *Conversely, every continuous decreasing traveling front that is locally absolutely continuous and satisfies $-U' > 0$ almost everywhere on its transition interval has*

$$Q'(p) = \frac{D(1-p)}{G(1-p)} \tag{S21}$$

almost everywhere and is recovered by (S18) up to translation.

In the original capacity variable, if v_p is determined by $S(v_p) = 1 - p$, then

$$Q'(p) = \frac{\Delta W\, \mathcal{D}(v_p)}{C(v_p)\, \mathcal{G}(v_p)}. \tag{S22}$$

Proof of Proposition S2. Positivity of η makes Q strictly increasing. On (a, b), $F(Q(p)) = p$, hence

$$F'(Q(p)) = \frac{1}{Q'(p)} = \frac{G(1-p)}{D(1-p)}.$$

With $U = 1 - F$ and $p = F(\xi) = 1 - U(\xi)$, this is $U' = -G(U)/D(U)$ and proves (S19). The inverse change of variables gives $\int_a^b F'(\xi)\, \mathrm{d}\xi = \int_0^1 \mathrm{d}p = 1$, so the constant completion is locally absolutely continuous and $\rho = F'$ has unit mass.

Because only $s \in (0, 1)$ is used here, a divergent endpoint limit of D is admissible. The quotient $\eta = D/G$ is continuous on the open interval by hypothesis, and Q never evaluates D at an endpoint.

For the weak equation, define $S(z, t) = U(z - ct - z_0)$. Where $0 < S < 1$, the flux identity in (S19) gives $j = L(S)$ directly. On a plateau, $S_z = 0$ and $G(S) = 0$, so the capillary term is assigned its continuous representative $G(S)$ and the same identity holds. Thus $j = L(S)$ everywhere after choosing that representative, and no separate endpoint limit of D is needed. Since $S \in W^{1,1}_{\mathrm{loc}}$ and L is affine, the Sobolev chain rule yields $S_t = -cS_z$ and $j_z = cS_z$ in distributions. Thus $S_t + j_z = 0$, which is exactly (S16). No interface Dirac mass occurs because the state and flux are continuous across each finite interface.

The support criterion follows directly from the endpoint limits in (S18), with the integrals interpreted as nonnegative improper Lebesgue integrals. For the converse, $Q' = 1/F'(Q) = -1/U'(Q)$. The traveling first integral gives $-U' = G(U)/D(U)$. Since $U(Q(p)) = 1 - p$, equation (S21) follows. Finally, $D = \mathcal{D}/C$ and $G = \mathcal{G}/\Delta W$ give (S22). ☐

Lemma S3 (Endpoint exponents and finite spatial moments)**.** *Let $\eta : (0, 1) \to (0, \infty)$ be locally integrable and suppose, for constants $C_{\mathrm{d}}, C_{\mathrm{w}} > 0$ and indices $b_{\mathrm{d}}, b_{\mathrm{w}} \in \mathbb{R}$,*

$$\eta(s) \sim C_{\mathrm{d}} s^{b_{\mathrm{d}}-1} \quad (s \downarrow 0), \qquad \eta(s) \sim C_{\mathrm{w}}(1-s)^{b_{\mathrm{w}}-1} \quad (s \uparrow 1). \tag{S23}$$

Define

$$Q^{\circ}(p) = \int_{1/2}^{p} \eta(1-r)\, \mathrm{d}r. \tag{S24}$$

Each exponent directly determines one endpoint. A positive value gives a finite interface, zero gives exponential approach, and a negative value gives an algebraic tail. More precisely, when $b_{\mathrm{d}} > 0$,

$$\xi_{\mathrm{d}} - Q^{\circ}(1-s) \sim \frac{C_{\mathrm{d}}}{b_{\mathrm{d}}} s^{b_{\mathrm{d}}}, \tag{S25}$$

and when $b_{\mathrm{d}} < 0$, $Q^{\circ}(1-s) = \Theta(s^{b_{\mathrm{d}}})$. The analogous statements hold at the wet endpoint with p and b_{w}. For every $1 \le r < \infty$, $Q^{\circ} \in L^r(0, 1)$ exactly when

$$b_{\mathrm{d}} > -\frac{1}{r}, \qquad b_{\mathrm{w}} > -\frac{1}{r}. \tag{S26}$$

Under these conditions, Q^{c} is defined and also belongs to $L^r(0, 1)$. The logarithmic boundary cases $b_{\mathrm{d}} = 0$ or $b_{\mathrm{w}} = 0$ belong to L^r for every finite r.

Proof of Lemma S3. At the dry endpoint, $p = 1 - s$ and $(Q^\circ)'(1-s) \sim C_\mathrm{d} s^{b_\mathrm{d}-1}$. Integration gives (S25) for $b_\mathrm{d} > 0$, a logarithm for $b_\mathrm{d} = 0$, and a multiple of s^{b_d} for $b_\mathrm{d} < 0$. The wet endpoint is identical after replacing s by $1-s$ and $1-p$ by p. Bounded and logarithmic quantiles lie in every finite L^r space, whereas an algebraic quantile satisfies $|Q^\circ|^r = \Theta(s^{rb})$, and

$$\int_0^\delta s^{rb}\,\mathrm{d}s < \infty \quad \iff \quad rb > -1.$$

This proves (S26) for Q°. The stated conditions imply $Q^\circ \in L^1(0,1)$, so Q^c is defined. Subtracting its finite mean does not alter endpoint integrability. □

S3.2 Hydraulic specializations

Standard VGM traveling-profile behavior near the dry and the saturated state has been examined before (Caputo and Stepanyants, 2008; Boakye-Ansah and Grassia, 2021, 2022). The theorem below states the endpoint exponents for that law together with the support and moment classes they imply. Theorem S5 then carries the same indices to the generalized family.

Theorem S4 (Standard VGM chord and endpoint specialization)**.** *Let $0 < m < 1$, $\alpha > 0$, $K_s > 0$, and $l \in \mathbb{R}$. For effective saturation $0 < s < 1$, define*

$$h_\alpha(s) = -\frac{1}{\alpha}\left(s^{-1/m} - 1\right)^{1-m}, \tag{S27}$$

$$A_m(s) = 1 - \left(1 - s^{1/m}\right)^m, \qquad k_r(s) = s^l A_m(s)^2, \tag{S28}$$

$$K(s) = K_s k_r(s), \qquad G(s) = K_s\{s - k_r(s)\}, \qquad D(s) = K(s) h'_\alpha(s). \tag{S29}$$

Then the following statements hold.

1. *The relative conductivity is nondecreasing on $(0,1)$ if and only if $l \geq -2/m$. If $l > -2/m$, it extends with $k_r(0) = 0$ and $k_r(1) = 1$.*

2. *The endpoint chord is strictly admissible,*

$$G(s) > 0 \quad (0 < s < 1), \tag{S30}$$

if and only if

$$l \geq l_{\mathrm{chord}}(m) := 1 - \frac{2}{m}. \tag{S31}$$

Under this condition, K is nonnegative and strictly increasing, with $K(0) = 0$ and $K(1) = K_s$. The ratio D/G therefore generates an exact front from $S = 1$ to $S = 0$. The front speed is K_s, and its flux is $K_s S$.

3. *Put*

$$b_\mathrm{d} := l + \frac{1}{m}, \qquad q := l + \frac{2}{m}. \tag{S32}$$

For every chord-admissible pair, the quantile stretch $\eta = D/G$ has the dry-end asymptotic

$$\eta(s) \sim C_\mathrm{d} s^{b_\mathrm{d}-1} \quad (s \downarrow 0), \qquad C_\mathrm{d} = \frac{m(1-m)}{\alpha}\begin{cases} 1, & q > 1, \\ (1-m^2)^{-1}, & q = 1, \end{cases} \tag{S33}$$

and the wet-end asymptotic

$$\eta(s) \sim C_{\mathrm{w}}(1-s)^{-2m} \quad (s \uparrow 1), \qquad C_{\mathrm{w}} = \frac{(1-m)m^{2m-1}}{2\alpha}. \tag{S34}$$

Consequently, the dry endpoint is compact, exponential, or algebraic according as $b_{\mathrm{d}} > 0$, $b_{\mathrm{d}} = 0$, or $b_{\mathrm{d}} < 0$. In the compact case,

$$U(\xi) \sim \left[\frac{b_{\mathrm{d}}}{C_{\mathrm{d}}}(\xi_{\mathrm{d}} - \xi)\right]^{1/b_{\mathrm{d}}} \quad (\xi \uparrow \xi_{\mathrm{d}}). \tag{S35}$$

In the algebraic case, $U(\xi) = \Theta(\xi^{-1/(-b_{\mathrm{d}})})$ as $\xi \to +\infty$, where $f = \Theta(g)$ means that f/g stays between two positive constants in the stated limit. The wet endpoint is compact, exponential, or algebraic according as $m < 1/2$, $m = 1/2$, or $m > 1/2$. In the compact case,

$$1 - U(\xi) \sim \left[\frac{1-2m}{C_{\mathrm{w}}}(\xi - \xi_{\mathrm{w}})\right]^{1/(1-2m)} \quad (\xi \downarrow \xi_{\mathrm{w}}). \tag{S36}$$

In the algebraic case, $1 - U(\xi) = \Theta(|\xi|^{-1/(2m-1)})$ as $\xi \to -\infty$.

4. *At fixed (m, l, K_s), changing the air-entry scale gives*

$$\eta_\alpha = \alpha^{-1}\eta_1, \qquad Q^\circ_\alpha = \alpha^{-1}Q^\circ_1, \qquad \ell_{p_1,p_2}(\alpha) = \alpha^{-1}\ell_{p_1,p_2}(1) \tag{S37}$$

for every interior interlevel width. Here ℓ_{p_1,p_2} is the spatial width between two interior probability levels. For every $1 \le r < \infty$, $Q^\circ_\alpha \in L^r(0,1)$ exactly when

$$b_{\mathrm{d}} > -\frac{1}{r}, \qquad m < \frac{r+1}{2r}. \tag{S38}$$

Under these conditions, Q^c_α exists, belongs to $L^r(0,1)$, and $Q^c_\alpha = \alpha^{-1}Q^c_1$. If μ^c_α denotes the law with this mean-centered quantile, then the one-dimensional r-Wasserstein distance W_r satisfies

$$W_r(\mu^c_{\alpha_1}, \mu^c_{\alpha_2}) = \left|\alpha_1^{-1} - \alpha_2^{-1}\right| \, \|Q^c_1\|_{L^r(0,1)}. \tag{S39}$$

In particular, $r = 2$ gives $b_{\mathrm{d}} > -1/2$ and $m < 3/4$.

Proof of Theorem S4. Set $x = s^{1/m}$ and $y = 1 - x$. Since $0 < m < 1$, concavity gives $(1-x)^m < 1 - mx$, whereas $(1-x)^m > 1 - x$, for $0 < x < 1$. Hence the global two-sided estimate

$$ms^{1/m} < A_m(s) < s^{1/m}, \qquad 0 < s < 1. \tag{S40}$$

Also

$$\frac{sA'_m(s)}{A_m(s)} = \frac{x(1-x)^{m-1}}{1-(1-x)^m}. \tag{S41}$$

The inequality $sA'_m/A_m > 1/m$ is equivalent to

$$my^{m-1} + (1-m)y^m > 1.$$

The left side equals 1 at $y = 1$ and has derivative $m(1-m)y^{m-2}(y-1) < 0$ on $(0,1)$. The left side is therefore strictly larger than 1 for $y < 1$. Combining this bound with (S41) gives

$$\frac{sk'_r(s)}{k_r(s)} = l + 2\frac{sA'_m(s)}{A_m(s)} > l + \frac{2}{m}. \tag{S42}$$

As $s \downarrow 0$, $A_m(s) \sim m s^{1/m}$, so $k_r(s) \sim m^2 s^{l+2/m}$ and the logarithmic derivative in (S42) tends to $l + 2/m$. This proves the sharp monotonicity threshold.

If $q = l + 2/m \geq 1$, (S40) gives $k_r(s) < s^q \leq s$, proving (S30). If $q < 1$, then $k_r(s)/s \sim m^2 s^{q-1} \to \infty$, so the chord is violated near the dry endpoint. This proves the necessary-and-sufficient condition (S31). The chord threshold also implies the preceding monotonicity condition.

Differentiating (S27) gives

$$h'_\alpha(s) = \frac{1-m}{\alpha m} s^{-1/m-1} \left(s^{-1/m} - 1\right)^{-m}. \tag{S43}$$

At the dry end, $h'_\alpha(s) \sim \alpha^{-1}(1-m)m^{-1}s^{-1/m}$ and $k_r(s) \sim m^2 s^q$. The chord gap satisfies $G(s)/K_s \sim s$ when $q > 1$, whereas $G(s)/K_s \sim (1-m^2)s$ when $q = 1$. These relations give (S33). At the wet end, with $\varepsilon = 1 - s$,

$$A_m(s) = 1 - m^{-m}\varepsilon^m + o(\varepsilon^m), \quad G(s) \sim 2K_s m^{-m}\varepsilon^m, \quad h'_\alpha(s) \sim \alpha^{-1}(1-m)m^{m-1}\varepsilon^{-m},$$

which gives (S34).

The support and profile statements now follow by integrating $Q'(p) = \eta(1-p)$. For example, at the dry end $\xi_\mathrm{d} - Q(1-s) \sim C_\mathrm{d} s^{b_\mathrm{d}}/b_\mathrm{d}$ when $b_\mathrm{d} > 0$, while $Q(1-s)$ grows logarithmically at $b_\mathrm{d} = 0$ and as s^{b_d} when $b_\mathrm{d} < 0$. The wet cases follow identically from $Q'(p) \sim C_\mathrm{w} p^{-2m}$.

Only h'_α depends on α, and it is proportional to α^{-1}. This proves (S37) after median anchoring. The dry exponent in (S33) is b_d. The wet exponent in (S34) is $b_\mathrm{w} = 1 - 2m$. Applying Lemma S3 gives $b_\mathrm{d} > -1/r$ and $1 - 2m > -1/r$, which is (S38). Under these conditions the mean is finite, so centering the scale identity gives (S39). □

Theorem S5 (Generalized VGM chord and endpoint criteria)**.** *Let $m > 0$, $n > 1$, $0 < \beta < n$, $\nu > 0$, $\alpha > 0$, $K_s > 0$, and $l \in \mathbb{R}$. Define the suction magnitude, normalized conductivity integral, relative conductivity, and diffusivity by*

$$H_{m,n}(s) = \frac{1}{\alpha}\left(s^{-1/m} - 1\right)^{1/n}, \qquad h_{m,n}(s) = -H_{m,n}(s), \tag{S44}$$

$$A_{m,n,\beta}(s) = \frac{\int_0^s H_{m,n}(t)^{-\beta}\,\mathrm{d}t}{\int_0^1 H_{m,n}(t)^{-\beta}\,\mathrm{d}t}, \qquad k_r(s) = s^l A_{m,n,\beta}(s)^\nu, \tag{S45}$$

$$K(s) = K_s k_r(s), \qquad D(s) = K(s) h'_{m,n}(s). \tag{S46}$$

Equations (S44)–(S46) define an established generalized conductivity class (Mualem and Dagan, 1978; Hoffmann-Riem et al., 1999; Kosugi, 1999). The independent-(m,n) VGM representation is also established (van Genuchten and Nielsen, 1985; Dourado Neto et al., 2011). Define

$$a = m + \frac{\beta}{n}, \qquad b = 1 - \frac{\beta}{n}, \qquad w = \frac{\beta}{mn}. \tag{S47}$$

Then

$$A_{m,n,\beta}(s) = I_{s^{1/m}}(a, b), \tag{S48}$$

where I_x is the regularized incomplete beta function, and the following statements hold.

1. *The conductivity is strictly increasing on $(0,1)$ if and only if*

$$l \geq -\nu(1 + w). \tag{S49}$$

If the inequality is strict, then $k_r(0) = 0$ and $k_r(1) = 1$. At equality, the dry limit is $[aB(a,b)]^{-\nu} \in (0,1)$.

2. *The full-endpoint chord is strictly admissible, $K_s\{s - k_r(s)\} > 0$ for $0 < s < 1$, if and only if*

$$l \geq 1 - \nu(1 + w). \tag{S50}$$

Under this condition the resulting front has speed K_s and flux $K_s S$.

3. *Under the chord condition, define*

$$b_\mathrm{d} = l + \nu(1 + w) - \frac{1}{mn} - 1, \qquad b_\mathrm{w} = \frac{1 + \beta}{n} - 1. \tag{S51}$$

For positive constants C_d and C_w,

$$\frac{D(s)}{K_s\{s - k_r(s)\}} \sim C_\mathrm{d} s^{b_\mathrm{d}-1} \quad (s \downarrow 0), \qquad \frac{D(s)}{K_s\{s - k_r(s)\}} \sim C_\mathrm{w}(1 - s)^{b_\mathrm{w}-1} \quad (s \uparrow 1). \tag{S52}$$

Each endpoint is compact, exponential, or algebraic according as its index is positive, zero, or negative. For $1 \leq r < \infty$, $Q^\circ \in L^r(0, 1)$ exactly when

$$b_\mathrm{d} > -\frac{1}{r}, \qquad b_\mathrm{w} > -\frac{1}{r}. \tag{S53}$$

Under these conditions, Q^c is defined and belongs to $L^r(0, 1)$. The median-anchored quantile and all interlevel widths are proportional to α^{-1}. The same scale law holds for Q^c whenever it is defined.

4. *The independent-(m, n) Mualem member $(\beta, \nu) = (1, 2)$ has*

$$l_\mathrm{chord} = -1 - \frac{2}{mn}, \qquad b_\mathrm{d} = l + 1 + \frac{1}{mn}, \qquad b_\mathrm{w} = \frac{2}{n} - 1. \tag{S54}$$

If $0 < m < 1$, $n = (1 - m)^{-1}$, and $\beta = 1$, then (S50) becomes the Kosugi outer-power boundary $l \geq 1 - \nu/m$. Taking $\nu = 2$ recovers Theorem S4.

Proof of Theorem S5. Put $x = s^{1/m}$. Substitution of $t = y^m$ in the numerator and denominator of (S45) gives

$$\int_0^s H_{m,n}(t)^{-\beta}\,\mathrm{d}t = m\alpha^\beta \int_0^x y^{a-1}(1 - y)^{b-1}\,\mathrm{d}y.$$

The common factor cancels on normalization, which proves (S48). Let $A(s) = I_x(a, b)$. Because $0 < b < 1$, the factor $(1 - y)^{b-1}$ is strictly increasing. Hence, for $0 < x < 1$,

$$I_x(a, b) < \frac{(1 - x)^{b-1} x^a}{aB(a, b)}, \qquad \frac{x\,\partial_x I_x(a, b)}{I_x(a, b)} > a.$$

The incomplete-beta bound gives

$$\frac{sA'(s)}{A(s)} > \frac{a}{m} = 1 + w, \qquad \lim_{s \downarrow 0} \frac{sA'(s)}{A(s)} = 1 + w. \tag{S55}$$

Integration of the strict logarithmic-slope inequality from s to 1 also gives

$$A(s) < s^{1+w}, \qquad A(s) \sim C_A s^{1+w}, \qquad C_A = \{aB(a, b)\}^{-1} \in (0, 1). \tag{S56}$$

The last strict range follows because $B(a, b) > \int_0^1 y^{a-1}\,\mathrm{d}y = 1/a$.

Write $q = l + \nu(1+w)$. Equations (S55)–(S56) give

$$\frac{sk_r'(s)}{k_r(s)} > q, \qquad k_r(s) \sim C_A^\nu s^q.$$

If $q \geq 0$, the first inequality is strict and K is strictly increasing. If $q < 0$, its logarithmic derivative is negative near zero. This proves (S49), including the nonzero dry limit when $q = 0$. If $q \geq 1$, then $k_r(s) < s^q \leq s$ on $(0,1)$. If $q < 1$, then $k_r(s)/s \sim C_A^\nu s^{q-1} \to \infty$. This proves the sharp chord condition (S50). The speed and flux then follow from the endpoint chord in Proposition S2.

Direct differentiation of (S44) gives

$$h_{m,n}'(s) = \frac{1}{\alpha mn} s^{-1/m-1}\left(s^{-1/m} - 1\right)^{1/n-1}. \tag{S57}$$

At the dry endpoint, $h_{m,n}'(s) \sim (\alpha mn)^{-1} s^{-1/(mn)-1}$ and $K(s) \sim K_s C_A^\nu s^q$. The chord gap is asymptotic to $K_s s$ for $q > 1$ and to $K_s(1 - C_A^\nu)s$ for $q = 1$. Thus D/G has dry exponent $q - 1/(mn) - 2 = b_\mathrm{d} - 1$.

For the wet endpoint, let $\delta = 1 - s$. Then

$$h_{m,n}'(s) \sim \frac{m^{-1/n}}{\alpha n}\delta^{1/n-1}, \qquad 1 - A(s) \sim \frac{m^{-b}}{bB(a,b)}\delta^b.$$

Since $0 < b < 1$, the beta-integral term dominates the order-δ change in s^l. Therefore

$$K_s\{s - k_r(s)\} \sim \frac{\nu K_s m^{-b}}{bB(a,b)}\delta^b,$$

and D/G has wet exponent $1/n - 1 - b = b_\mathrm{w} - 1$. Both asymptotic constants are positive. Lemma S3 now proves the support and moment statements. The normalized A, and hence K, is independent of α, whereas (S57) is proportional to α^{-1}. This proves the stated scale laws.

For $(\beta, \nu) = (1, 2)$, direct substitution gives (S54). If $n = (1-m)^{-1}$ and $\beta = 1$, then $1 + w = 1/m$, so the chord boundary is $l \geq 1 - \nu/m$. The case $\nu = 2$ agrees with Theorem S4. ☐

The statements below are consequences of the affine form of the chord boundary. The extrema over convex sets, the dual-norm distance, and the metric projection are standard convex analysis applied to that boundary.

Proposition S6 (Affine chord margins, repairs, and violation scales)**.** *For the generalized class in Theorem S5, let $x = (w, l)^\top$, $a_\nu = (\nu, 1)^\top$, and define*

$$\Delta_\nu(x) = l - 1 + \nu(1+w) = a_\nu^\top x + \nu - 1. \tag{S58}$$

Let $\mathcal{C}$ be a nonempty compact convex set and let $h_\mathcal{C}(v) = \max_{x\in\mathcal{C}} v^\top x$. The exact margin range is

$$\Delta_{\min} = -h_\mathcal{C}(-a_\nu) + \nu - 1, \qquad \Delta_{\max} = h_\mathcal{C}(a_\nu) + \nu - 1. \tag{S59}$$

Thus all represented laws are admissible when $\Delta_{\min} \geq 0$. No represented law is admissible when $\Delta_{\max} < 0$. Otherwise, the set intersects the chord boundary and contains laws on both sides or on the boundary. For a segment, the extrema occur at its endpoints. For an ellipsoid $\{\bar{x} + B_\mathrm{e} y : \|y\|_2 \leq r_\mathrm{e}\}$ with shape matrix B_e and radius r_e, they are $\Delta_\nu(\bar{x}) \mp r_\mathrm{e}\|B_\mathrm{e}^\top a_\nu\|_2$.

For any norm with dual norm $\|\cdot\|_*$, the exact classification radius at x_0 is

$$\rho_*(x_0) = \frac{|\Delta_\nu(x_0)|}{\|a_\nu\|_*}. \tag{S60}$$

The smallest common nonnegative shift of l that makes $\mathcal{C}$ admissible is

$$\delta_{\mathcal{C}} = (-\Delta_{\min})_+, \qquad K(s) \longmapsto s^{\delta_{\mathcal{C}}} K(s). \tag{S61}$$

For the constrained outer-power slice $n = (1-m)^{-1}$ and $\beta = 1$, put $u = 1/m$ and $\Delta_\nu = l-1+\nu u$. If $\varepsilon = -\Delta_\nu > 0$, then

$$m^\nu s^{-\varepsilon} < \frac{k_r(s)}{s} < s^{-\varepsilon}, \qquad 0 < s \le S_\star := m^{\nu/\varepsilon} \implies k_r(s) > s. \tag{S62}$$

The least exponent repair is $\widehat{l} = l + \varepsilon$ and satisfies $\widehat{K}/K = s^\varepsilon$. For standard VGM, the Euclidean radius in (u, l) is

$$\rho_*(m, l) = \frac{|l - 1 + 2/m|}{\sqrt{5}}. \tag{S63}$$

Proof of Proposition S6. The chord condition in Theorem S5 is equivalent to $\Delta_\nu \ge 0$. Since this margin is affine, its maximum over $\mathcal{C}$ is $h_{\mathcal{C}}(a_\nu) + \nu - 1$ and its minimum is $-h_{\mathcal{C}}(-a_\nu) + \nu - 1$. Compactness ensures that both extrema are attained. Convexity and continuity give the crossing case. The segment result is immediate, and Cauchy–Schwarz gives the ellipsoid extrema.

If a parameter displacement δx reaches the classification boundary, then $a_\nu^\top \delta x = -\Delta_\nu(x_0)$. Hölder duality gives

$$|\Delta_\nu(x_0)| \le \|a_\nu\|_* \|\delta x\|.$$

In finite dimension a unit vector attaining the dual norm exists. Scaling that vector reaches equality, which proves (S60). A common shift δ of l adds δ to every margin. The least nonnegative shift is therefore $(-\Delta_{\min})_+$, and the factor s^l in K changes by s^δ.

On the constrained slice, $1 + w = 1/m$. If $\varepsilon = -\Delta_\nu > 0$, then $l - 1 = -\nu/m - \varepsilon$. The standard bound $m s^{1/m} < A_m(s) < s^{1/m}$ gives

$$m^\nu s^{-\varepsilon} < \frac{k_r(s)}{s} < s^{-\varepsilon}.$$

For $s \le m^{\nu/\varepsilon}$, the strict lower bound is at least one. Increasing l by ε is the least repair and multiplies K by s^ε. Finally, standard VGM has $a_2 = (2,1)^\top$, whose Euclidean norm is $\sqrt{5}$, proving (S63). $\square$

The Brooks–Corey retention law and its Mualem conductivity form are established (Brooks and Corey, 1964; Mualem, 1976). The corollary below places that law in the endpoint and moment classification.

Corollary S7 (Brooks–Corey support and scale law)**.** *Let $\lambda > 0$, $h_b > 0$, $K_s > 0$, and $\gamma > 1$, and define*

$$h(s) = -h_b s^{-1/\lambda}, \qquad K(s) = K_s s^\gamma, \qquad G(s) = K_s(s - s^\gamma). \tag{S64}$$

Then $G > 0$ on $(0,1)$ and

$$\eta(s) = \frac{D(s)}{G(s)} = \frac{h_b}{\lambda} \frac{s^{\gamma - 1/\lambda - 2}}{1 - s^{\gamma - 1}}. \tag{S65}$$

Put $b_{\mathrm{d}} = \gamma - 1 - 1/\lambda$. The dry endpoint is compact, exponential, or algebraic according as $b_{\mathrm{d}} > 0$, $b_{\mathrm{d}} = 0$, or $b_{\mathrm{d}} < 0$, with the same powers as in Theorem S4. The wet endpoint is exponential for every admissible parameter set, since $\eta(s) \sim h_b[\lambda(\gamma-1)]^{-1}(1-s)^{-1}$. For $1 \le r < \infty$, $Q^\circ \in L^r(0,1)$ exactly when $b_{\mathrm{d}} > -1/r$. The median-anchored quantile and all interlevel widths scale linearly with

h_b. Under this moment condition, Q^c is defined, belongs to $L^r(0,1)$, and obeys the same scale law. For the common Mualem–Brooks–Corey exponent $\gamma = l + 2 + 2/\lambda$, dry compactness is exactly

$$l > -1 - \frac{1}{\lambda}. \tag{S66}$$

Proof of Corollary S7. The chord condition follows from $s^\gamma < s$. Direct differentiation of h and cancellation of K_s give (S65). Its dry asymptotic is $(h_b/\lambda)s^{b_\mathrm{d}-1}$, and its wet asymptotic follows from $1 - s^{\gamma-1} \sim (\gamma-1)(1-s)$. Proposition S2 gives the support classification. Lemma S3 gives the moment condition and the conditional statement for Q^c. Linearity in h_b follows from $\eta \propto h_b$. Substitution of the Mualem exponent gives (S66). □

S3.3 Finite endpoints and pressure caps

Parts 1 to 3 below record the established criterion for traveling connections between arbitrary interior states (Witelski, 1997, 2005; Gilding and Kersner, 1996; Caputo and Stepanyants, 2008). They are restated with one-sided endpoint hypotheses that the generalized VGM laws satisfy. Parts 4 and 5 apply that criterion to a retention-selected dry state and to a fixed saturation floor.

Theorem S8 (Selected-endpoint criterion with pressure-head applications)**.** *Let $0 \le s_\mathrm{d} < s_\mathrm{w} \le 1$, let $K \in C([s_\mathrm{d}, s_\mathrm{w}]) \cap C^1((s_\mathrm{d}, s_\mathrm{w}))$, and let D be continuous and positive on the open endpoint interval. Differentiability is assumed only on the open interval, because K' diverges at $s_\mathrm{w} = 1$ for the generalized VGM laws classified above. Define*

$$c_{\mathrm{d,w}} = \frac{K(s_\mathrm{w}) - K(s_\mathrm{d})}{s_\mathrm{w} - s_\mathrm{d}}, \quad L_{\mathrm{d,w}}(s) = K(s_\mathrm{d}) + c_{\mathrm{d,w}}(s - s_\mathrm{d}), \quad G_{\mathrm{d,w}} = L_{\mathrm{d,w}} - K. \tag{S67}$$

The following statements hold.

1. *A continuous decreasing front from s_w to s_d exists with positive diffusivity exactly when*

$$G_{\mathrm{d,w}}(s) > 0 \qquad (s_\mathrm{d} < s < s_\mathrm{w}). \tag{S68}$$

   The front speed is $c_{\mathrm{d,w}}$, the flux is $L_{\mathrm{d,w}}(S)$, and the normalized front quantile satisfies

$$Q'_{\mathrm{d,w}}(p) = \frac{(s_\mathrm{w} - s_\mathrm{d})D\{s_\mathrm{w} - (s_\mathrm{w} - s_\mathrm{d})p\}}{G_{\mathrm{d,w}}\{s_\mathrm{w} - (s_\mathrm{w} - s_\mathrm{d})p\}}, \qquad 0 < p < 1. \tag{S69}$$

2. *Let*

$$\mathcal{R}_{\mathrm{d,w}} = \{s \in (s_\mathrm{d}, s_\mathrm{w}) : K'(s) = c_{\mathrm{d,w}}\}. \tag{S70}$$

   Condition (S68) holds exactly when $G_{\mathrm{d,w}}(s_*) > 0$ for every $s_* \in \mathcal{R}_{\mathrm{d,w}}$. If the stationary set is finite, an analytical conductivity derivative therefore reduces the whole-interval condition to finitely many scalar evaluations.

3. *Each endpoint rate below requires finite one-sided limits of both D and K' at that endpoint alone. Suppose that $D(s) \to D_\mathrm{d} \in (0,\infty)$ and $K'(s) \to K'_\mathrm{d} \in \mathbb{R}$ as $s \downarrow s_\mathrm{d}$. If $c_{\mathrm{d,w}} > K'_\mathrm{d}$, the dry endpoint is approached exponentially with rate $(c_{\mathrm{d,w}} - K'_\mathrm{d})/D_\mathrm{d}$. Suppose instead that $D(s) \to D_\mathrm{w} \in (0,\infty)$ and $K'(s) \to K'_\mathrm{w} \in \mathbb{R}$ as $s \uparrow s_\mathrm{w}$. If $c_{\mathrm{d,w}} < K'_\mathrm{w}$, the wet endpoint is also exponential, with rate $(K'_\mathrm{w} - c_{\mathrm{d,w}})/D_\mathrm{w}$. For generalized VGM at $s_\mathrm{w} = 1$, these finite-limit assumptions fail. The wet endpoint index in Theorem S5 gives the classification instead.*

4. *A finite dry cap $h \geq h_{\mathrm{cap}}$ with $h_{\mathrm{cap}} < 0$ in the generalized VGM retention law selects*

$$s_{\mathrm{d}} = S_{\mathrm{cap}} = \left[1 + (\alpha|h_{\mathrm{cap}}|)^n\right]^{-m}. \tag{S71}$$

For $s_{\mathrm{w}} = 1$, its exact wave speed is

$$c_{\mathrm{cap},1} = K_s \widehat{c}_{\mathrm{cap},1}, \qquad \widehat{c}_{\mathrm{cap},1} = \frac{1 - k_r(S_{\mathrm{cap}})}{1 - S_{\mathrm{cap}}}. \tag{S72}$$

The cap-selected wave is therefore not a clipped copy of the full-endpoint wave. When the critical set is finite, equation (S70) decides admissibility through the generalized VGM derivative. Because $K(s) = K_s k_r(s)$, that critical set is $\{s : k_r'(s) = \widehat{c}_{\mathrm{cap},1}\}$ and the sign of $G_{\mathrm{cap},1}/K_s$ decides the classification. The classification is thus independent of K_s, while the speed is proportional to it.

5. *Let $0 < |\Omega| < \infty$. If a numerical state satisfies $S_{\mathrm{num}} \geq S_{\mathrm{cap}}$ and a full-endpoint reference state satisfies $S^* = 0$ on a measurable set $A_{\mathrm{d}} \subset \Omega$ of positive measure, then, for $1 \leq r < \infty$,*

$$\|S_{\mathrm{num}} - S^*\|_{L^\infty(\Omega)} \geq S_{\mathrm{cap}}, \qquad \left(|\Omega|^{-1} \int_\Omega |S_{\mathrm{num}} - S^*|^r \,\mathrm{d}z\right)^{1/r} \geq S_{\mathrm{cap}} \left(\frac{|A_{\mathrm{d}}|}{|\Omega|}\right)^{1/r}. \tag{S73}$$

The bounds in (S73) persist under mesh and time-step refinement at fixed cap.

For a target floor $0 < \tau < 1$, direct inversion gives

$$|h_{\mathrm{cap}}| \geq H_\tau^{\mathrm{VG}} = \frac{1}{\alpha}\left(\tau^{-1/m} - 1\right)^{1/n}, \qquad |h_{\mathrm{cap}}| \geq H_\tau^{\mathrm{BC}} = h_b \tau^{-1/\lambda}. \tag{S74}$$

The first formula covers independent m and n, whereas the second covers the Brooks–Corey law in Corollary S7.

Proof of Theorem S8. For a traveling state $U(z - ct)$, one integration of the conservation law gives an affine flux $K(s_{\mathrm{d}}) + c(U - s_{\mathrm{d}})$. Evaluation at s_{w} fixes $c = c_{\mathrm{d,w}}$, and the first integral becomes

$$D(U)U' = -G_{\mathrm{d,w}}(U). \tag{S75}$$

Thus a decreasing front with positive D requires the strict chord gap. Conversely, when the gap is positive, integration of $D/G_{\mathrm{d,w}}$ constructs the monotone profile, with constant completion at either finite interface. The resulting profile is the rescaled construction in Proposition S2. For $p = (s_{\mathrm{w}} - U)/(s_{\mathrm{w}} - s_{\mathrm{d}})$, inversion of (S75) gives (S69).

The gap vanishes at both endpoints and satisfies $G_{\mathrm{d,w}}' = c_{\mathrm{d,w}} - K'$. Positivity on the open interval therefore implies positivity at every point of $\mathcal{R}_{\mathrm{d,w}}$. Conversely, if the gap is nonpositive at an interior point, its minimum is attained at an interior point and is nonpositive. The interior minimizer belongs to $\mathcal{R}_{\mathrm{d,w}}$.

Near the dry endpoint, continuity of K and the one-sided limit $K'(s) \to K_{\mathrm{d}}'$ give that one-sided derivative by the mean value theorem. Hence

$$G_{\mathrm{d,w}}(s) = \{c_{\mathrm{d,w}} - K_{\mathrm{d}}'\}(s - s_{\mathrm{d}}) + o(s - s_{\mathrm{d}}).$$

With the finite positive limit D_{d}, equation (S75) gives exponential approach at the stated rate. The wet expansion is analogous, with coefficient $K_{\mathrm{w}}' - c_{\mathrm{d,w}}$ and limit D_{w}. Only the endpoint being classified enters either expansion, so neither requires a limit at the other endpoint. When $s_{\mathrm{w}} = 1$ in the generalized VGM class, both D and K' diverge there and the wet asymptotics in Theorem S5 apply instead.

Solving (S44) for the state at h_{cap} gives (S71). Substitution of $K(1) = K_s$ and $K(S_{\text{cap}}) = K_s k_r(S_{\text{cap}})$ into the secant definition gives (S72). For the representation bound, on the positive-measure set A_{d} one has $|S_{\text{num}} - S^*| = S_{\text{num}} \geq S_{\text{cap}}$. Taking the essential supremum or integrating its rth power proves (S73). The bound depends only on the fixed state floor, so refinement cannot remove it. Finally, direct inversion of the generalized VGM and Brooks–Corey retention relations gives (S74). □

References

Y. A. Boakye-Ansah and P. Grassia. Comparing and contrasting travelling wave behaviour for groundwater flow and foam drainage. *Transport in Porous Media*, 137:255–280, 2021. doi: 10.1007/s11242-021-01562-w.

Y. A. Boakye-Ansah and P. Grassia. Sensitivity of travelling wave solution to Richards equation to soil material property functions. *Transport in Porous Media*, 145:789–812, 2022. doi: 10.1007/s11242-022-01878-1.

P. Broadbridge and I. White. Constant rate rainfall infiltration: A versatile nonlinear model: 1. analytic solution. *Water Resources Research*, 24(1):145–154, 1988. doi: 10.1029/WR024i001p00145.

R. H. Brooks and A. T. Corey. Hydraulic properties of porous media. Hydrology Paper 3, Colorado State University, Fort Collins, Colorado, 1964.

R. H. Byrd, P. Lu, J. Nocedal, and C. Zhu. A limited memory algorithm for bound constrained optimization. *SIAM Journal on Scientific Computing*, 16(5):1190–1208, 1995. doi: 10.1137/0916069.

J.-G. Caputo and Y. A. Stepanyants. Front solutions of Richards' equation. *Transport in Porous Media*, 74 (1):1–20, 2008. doi: 10.1007/s11242-007-9180-x.

D. Dourado Neto, Q. de Jong van Lier, M. T. van Genuchten, K. Reichardt, K. Metselaar, and D. R. Nielsen. Alternative analytical expressions for the general van Genuchten–Mualem and van Genuchten–Burdine hydraulic conductivity models. *Vadose Zone Journal*, 10(2):618–623, 2011. doi: 10.2136/vzj2009.0191.

B. H. Gilding. Qualitative mathematical analysis of the Richards equation. *Transport in Porous Media*, 6 (5–6):651–666, 1991. doi: 10.1007/BF00137854.

B. H. Gilding and R. Kersner. The characterization of reaction–convection–diffusion processes by travelling waves. *Journal of Differential Equations*, 124(1):27–79, 1996. doi: 10.1006/jdeq.1996.0002.

Brian H. Gilding and Robert Kersner. *Travelling Waves in Nonlinear Diffusion-Convection Reaction*, volume 60 of *Progress in Nonlinear Differential Equations and Their Applications*. Birkhäuser, Basel, 2004. doi: 10.1007/978-3-0348-7964-4.

H. Hoffmann-Riem, M. Th. van Genuchten, and H. Flühler. A general model of the hydraulic conductivity of unsaturated soils. In M. Th. van Genuchten, F. J. Leij, and L. Wu, editors, *Characterization and Measurement of the Hydraulic Properties of Unsaturated Porous Media*, pages 31–42. University of California, Riverside, California, 1999.

Fredrik Johansson. Arb: Efficient arbitrary-precision midpoint-radius interval arithmetic. *IEEE Transactions on Computers*, 66(8):1281–1292, 2017. doi: 10.1109/TC.2017.2690633.

Benjamin Jourdain and Julien Reygner. Propagation of chaos for rank-based interacting diffusions and long time behaviour of a scalar quasilinear parabolic equation. *Stochastic Partial Differential Equations: Analysis and Computations*, 1(3):455–506, 2013. doi: 10.1007/s40072-013-0014-2.

K. Kosugi. General model for unsaturated hydraulic conductivity for soils with lognormal pore-size distribution. *Soil Science Society of America Journal*, 63(2):270–277, 1999. doi: 10.2136/sssaj1999.03615995006300020003x.

Ramon E. Moore, R. Baker Kearfott, and Michael J. Cloud. *Introduction to Interval Analysis*. Society for Industrial and Applied Mathematics, Philadelphia, Pennsylvania, 2009. doi: 10.1137/1.9780898717716.

Y. Mualem. A new model for predicting the hydraulic conductivity of unsaturated porous media. *Water Resources Research*, 12(3):513–522, 1976. doi: 10.1029/WR012i003p00513.

Y. Mualem and G. Dagan. Hydraulic conductivity of soils: Unified approach to the statistical models. *Soil Science Society of America Journal*, 42(3):392–395, 1978. doi: 10.2136/sssaj1978.03615995004200030003x.

M. J. D. Powell. An efficient method for finding the minimum of a function of several variables without calculating derivatives. *The Computer Journal*, 7(2):155–162, 1964. doi: 10.1093/comjnl/7.2.155.

M. Th. van Genuchten and D. R. Nielsen. On describing and predicting the hydraulic properties of unsaturated soils. *Annales Geophysicae*, 3(5):615–628, 1985.

M. Weynants, L. Montanarella, G. Tóth, et al. European HYdropedological data inventory (EU-HYDI). Technical Report EUR 26053 EN, JRC81129, European Commission, Joint Research Centre, Luxembourg, 2013. https://publications.jrc.ec.europa.eu/repository/handle/JRC81129.

T. P. Witelski. Perturbation analysis for wetting fronts in Richard's equation. *Transport in Porous Media*, 27 (2):121–134, 1997. doi: 10.1023/A:1006513009125.

T. P. Witelski. Motion of wetting fronts moving into partially pre-wet soil. *Advances in Water Resources*, 28 (10):1133–1141, 2005. doi: 10.1016/j.advwatres.2004.06.006.

V. A. Zlotnik, T. Wang, J. L. Nieber, and J. Šimůnek. Verification of numerical solutions of the Richards equation using a traveling wave solution. *Advances in Water Resources*, 30(9):1973–1980, 2007. doi: 10.1016/j.advwatres.2007.03.008.